ChemistryOpen

Research Article
doi.org/10.1002/open.202200197

Chemistry Europe
European Chemical Societies Publishing

www.chemistryopen.org

Structure and Conformation of Novel BODIPY Ugi Adducts

Ismael Javier Arroyo-Córdoba,[a] Gonzalo Gamboa-Velázquez,[a] Claudia Gabriela Avila-Ortiz,[a] Marco A. Leyva-Ramírez,[a] María Teresa Cortez-Picasso,[a] Marco A. García-Revilla,[b] Diana E. Ramírez-Ornelas,[b] Eduardo Peña-Cabrera,*[b] and Eusebio Juaristi*[a, c]

Two novel BODIPY-Ugi (boron dipyrromethene) adducts exhibit peculiar room temperature (T = 20 °C) H-1 NMR spectra in that several protons located at the aromatic aniline-type ring are lost in the baseline. This observation revealed the existence of a dynamic conformational process where rotation around the C–N bond is hindered. Variable-temperature H-1 and C-13 NMR spectroscopic analysis confirmed this conclusion; that is, low-temperature spectra show distinct signals for all four aromatic protons below coalescence, whereas average signals are recorded above coalescence (T = +120 °C). Particularly interesting was the rather large difference in chemical shifts for the *ortho* protons below coalescence, $\Delta\delta = 1.45$ ppm, which was explained based on DFT computational analysis. Indeed, the calculated lowest-energy gas-phase conformation of the BODIPY Ugi adducts locates one half of the aniline-type ring in the shielding anisotropic cone of the bridge phenyl ring in the BODIPY segment. This is in contrast to the solid-state conformation established by X-ray diffraction analysis that shows a nearly parallel arrangement of the aromatic rings, probably induced by crystal packing forces.

Introduction

In recent years, boron dipyrromethene (BODIPY) dyes have attracted extraordinary interest from the scientific community owing to their excellent photophysical properties, including strong absorption and emission in their optical spectra, large molar extinction coefficients, and high fluorescence quantum yields.[1–4] Indeed, BODIPY dyes have been successfully applied as markers in living cell bioimaging,[5] in fluorescence sensing,[6] in photodynamic therapy,[7] and in dye-sensitized solar cells,[8] to highlight a few applications. It is therefore not surprising that several synthetic strategies are currently being developed to obtain compounds that incorporate BODIPY fragments in their structure.[9]

Among the most efficient synthetic strategies that afford a wide variety of BODIPY-type compounds, one can highlight the Liebeskind-Srogl coupling reaction[10] as a very convenient strategy for derivatization of the Biellmann BODIPY at the 8 position (Scheme 1).

In this regard, Peña-Cabrera and coworkers have taken advantage of the procedure in the design and synthesis of a variety of novel BODIPY derivatives.[11–14] Furthermore, Juaristi, Peña-Cabrera, and coworkers reported the successful use of mechanochemical activation to carry out the Liebeskind-Srogl reaction in good yields under solvent-free sustainable conditions.[15]

On the other hand, the Ugi reaction is one of the most studied multicomponent reactions.[16–20] In this regard, in 2015, Polindara and Juaristi reported the use of mechanochemistry to successfully carry out this reaction for a variety of substrates (Scheme 2).[21]

In a particular application of this mechanochemical procedure, several formyl-functionalized BODIPY dyes were recently prepared and evaluated by flow cytometry and fluorescence microscopy, providing evidence that the novel dyes efficiently

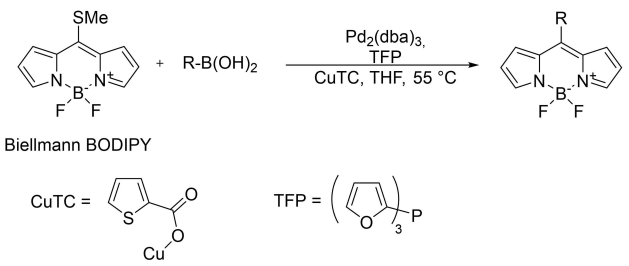

Scheme 1. Liebeskind-Srogl coupling reaction in the functionalization of the Biellmann BODIPY.

[a] Dr. I. J. Arroyo-Córdoba, G. Gamboa-Velázquez, Dr. C. G. Avila-Ortiz, M. A. Leyva-Ramírez, M. T. Cortez-Picasso, Prof. Dr. E. Juaristi
Department of Chemistry
Centro de Investigación y de Estudios Avanzados
Avenida IPN 2508
San Pedro Zacatenco
07360 Ciudad de México (Mexico)
E-mail: ejuarist@cinvestav.mx

[b] Prof. Dr. M. A. García-Revilla, D. E. Ramírez-Ornelas, Prof. Dr. E. Peña-Cabrera
Department of Chemistry
Universidad de Guanajuato
Noria Alta S/N
36050 Guanajuato, Gto. (Mexico)
E-mail: eduardop@ugto.mx

[c] Prof. Dr. E. Juaristi
El Colegio Nacional
Luis González Obregón 23
Centro Histórico
06020 Ciudad de México (Mexico)

Supporting information for this article is available on the WWW under https://doi.org/10.1002/open.202200197

© 2022 The Authors. Published by Wiley-VCH GmbH. This is an open access article under the terms of the Creative Commons Attribution Non-Commercial NoDerivs License, which permits use and distribution in any medium, provided the original work is properly cited, the use is non-commercial and no modifications or adaptations are made.

© 2022 The Authors. Published by Wiley-VCH GmbH

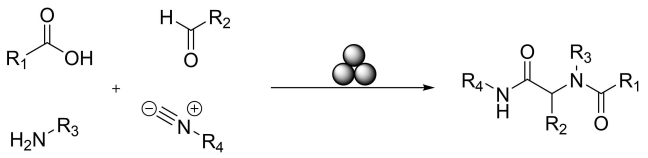

Scheme 2. Multicomponent (4MC) Ugi reaction performed under mechanochemical activation.

stain peripheral blood mononuclear cells.[22] Compounds **A-1** and **A-2** were obtained following the previously reported methodology using mechanochemical activation (Scheme 3).[22] Both compounds exhibited a Φ (fluorescence quantum yield) value of 0.03.

Interestingly, NMR-spectroscopic observations provided evidence that the novel BODIPY Ugi adducts participate in dynamic conformational processes that were deemed to deserve further attention, especially in view of several recent conformational studies with related aniline-derived compounds.[23–25] Interestingly, a series of Ugi adducts reported previously by our research group did not show this dynamic effect.[21] By the same token, the work reported by Ogawa and coworkers, which describes structurally related derivatives not containing the BODIPY core (Figure 1), did not exhibit such dynamic behavior.[26]

Accordingly, it was decided to carry out a complementary structural analysis of the novel BODIPY Ugi adducts **A-1** and **A-2** by means of X-ray diffraction analysis, variable temperature NMR spectroscopy including two-dimension NMR techniques (COSY, HSQC, HMBC), as well as quantum molecular modeling (DFT), which would allow us to understand the conformational behavior of such BODIPY Ugi adducts.

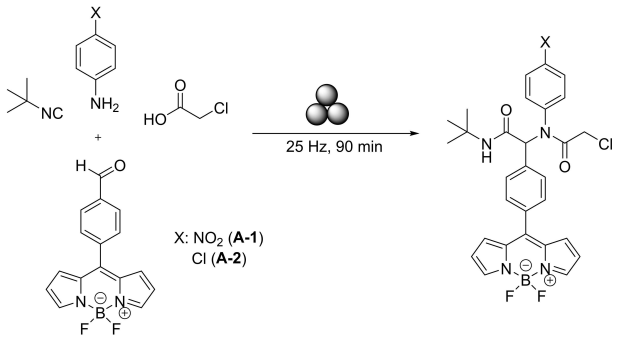

Scheme 3. Ugi reaction for the preparation of BODIPY adducts **A-1** and **A-2**.[22]

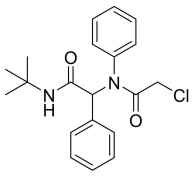

Ogawa et al. (2019), ref. 26

Figure 1. Ogawa's Ugi adduct not exhibiting hindered ring rotation.

Results and Discussion

*H-1 and C-13 NMR characterization of **A-1** (p-nitro)-substituted and **A-2** (p-chloro)-substituted BODIPY Ugi adducts.*

Figure 2 presents the room temperature (20 °C) proton and carbon-13 NMR signal assignments for *p*-nitro Ugi adduct **A-1** in $CDCl_3$. Interestingly, a simple signal at 8.05 ppm could be assigned to the two aromatic hydrogen atoms that are in *ortho* position to the nitro group in the aniline-type ring. (This assignment was confirmed by HSQC correlation). Nevertheless, the signal corresponding to the hydrogen atoms in *meta* position to the nitro group was not observed.

On the other hand, the appearance of a rather broad signal at 7.2 ppm suggested that a dynamic process is taking place, provoking the disappearance of some signals at room temperature. Indeed, when the temperature of measurement was lowered, the missing signals could be observed (see below).

COSY 2DNMR experiments were performed to securely assign the protons on the aniline-type ring. At room temperature (20 °C), compound **A-1** presented a simple signal at 8.06 ppm integrating for two hydrogen atoms and correlating only with itself. As the recording temperature was lowered, this signal coalesced at ca. −20 °C to reappear at lower temperature with a chemical shift equal to 8.17 ppm.

The fact that this signal at 8.17 ppm, which is a singlet, only correlates with itself (Figure 3), indicates that both protons are on the same side of the aromatic ring and afford the same chemical shift. On the other hand, the signal observed at 7.87 ppm correlated with the doublet at 6.72 ppm, which means that these protons are located *vicinally* to each other. In contrast, when the COSY 2DNMR experiment was performed at +120 °C in DMSO-d6 (Figure 4), the correlation pattern is in line with a typical A_2B_2 system affording two doublets at 8.0 ppm and 7.6 ppm that correlate with each other.

In this context, HMBC 2DNMR spectra (see Supporting Information) permitted unequivocal H-1 and C-13 assignments for BODIPY Ugi adduct **A-2** (Figure 5). In this case, the signals

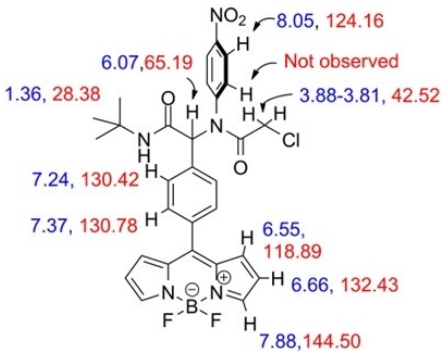

Figure 2. ^{1}H (blue) and ^{13}C (red) NMR chemical shifts recorded for Ugi adduct **A-1** at room temperature (20 °C) in $CDCl_3$.

© 2022 The Authors. Published by Wiley-VCH GmbH

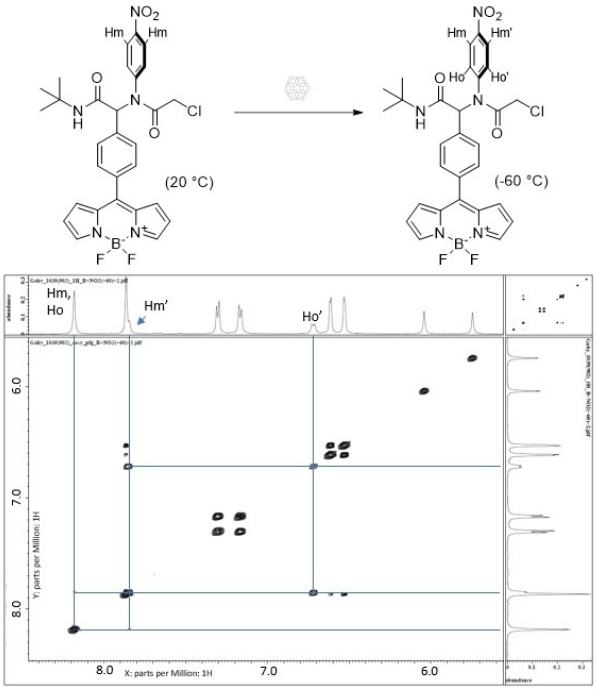

Figure 3. COSY 2DNMR spectra recorded at −60 °C in CD_2Cl_2.

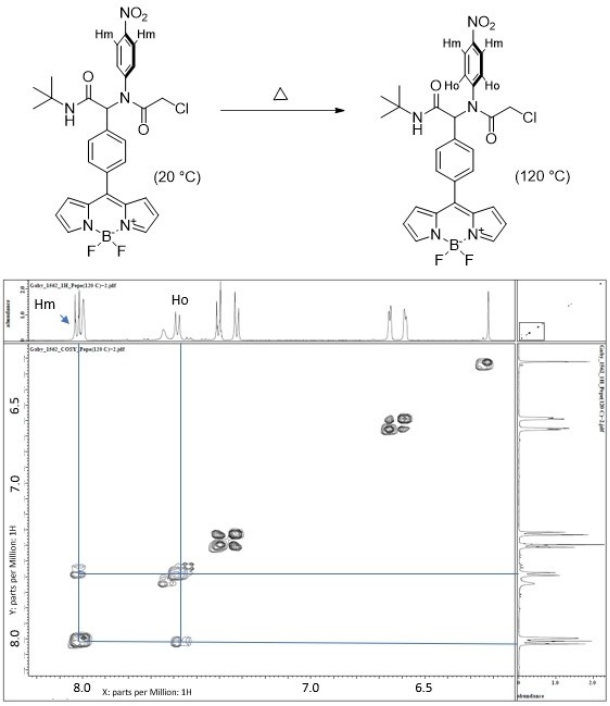

Figure 4. COSY 2DNMR spectra recorded at +120 °C in DMSO-d_6.

corresponding to the four hydrogen atoms in the aniline segment were not observed at 20 °C (room temperature).

As also the case for Ugi adduct **A-1** (see above), the low-temperature (−60 °C) COSY 2DNMR spectrum of adduct **A-2** exhibited four distinct signals that were ascribed to the four protons on the aniline type ring (Figure 6). Each of these signals

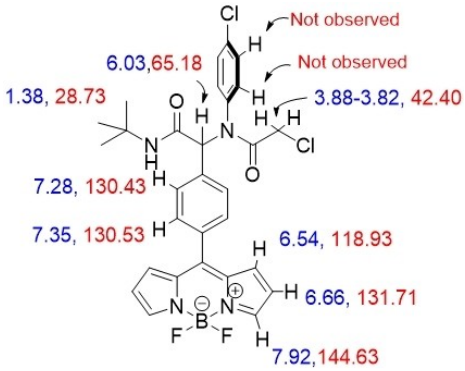

Figure 5. ^{1}H (blue) and ^{13}C (red) NMR signal assignment of compound **A-2** at 20 °C.

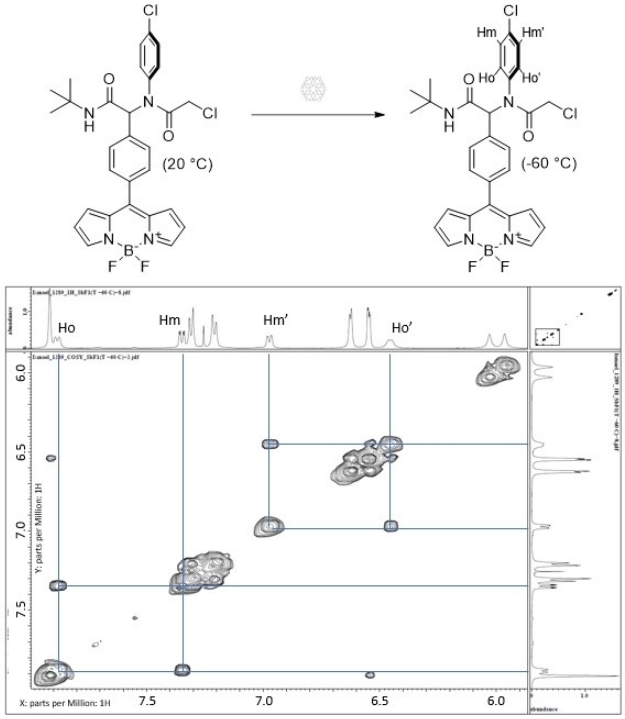

Figure 6. COSY 2DNMR spectra recorded at −60 °C in $CDCl_3$.

integrated for one proton. The doublet at 7.89 ppm correlated with itself as well as with a signal at 7.35 ppm, indicating that these protons are in *vicinal* position to each other. On the other hand, the doublet at 6.96 ppm presented a correlation with itself and with a doublet signal at 6.46 ppm, which means that these protons are *vicinal* to each other. Thus, all four protons at the aniline-type aromatic ring could be differentiated and identified (Figure 7). HSQC and HMBC 2DNMR spectra (see Supporting Information) permitted the unequivocal assignment of all H-1 and C-13 signals.

© 2022 The Authors. Published by Wiley-VCH GmbH

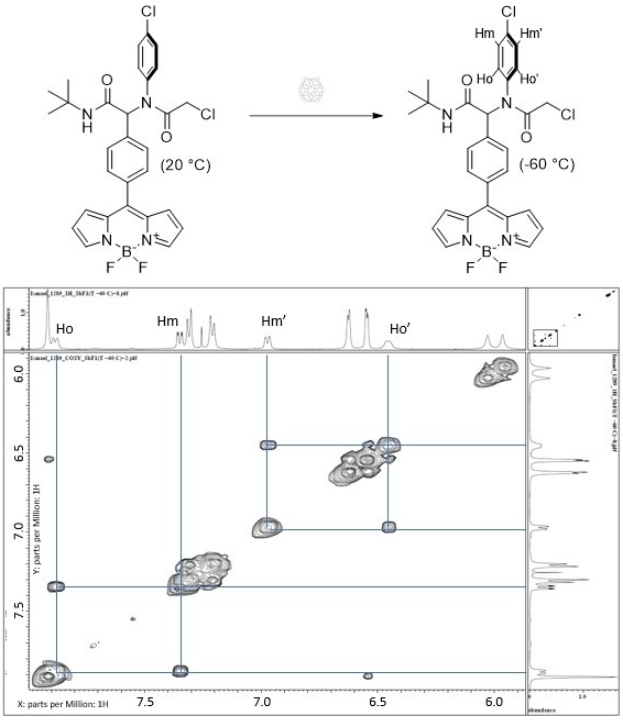

Figure 7. COSY 2DNMR spectra recorded at +120 °C in DMSO-d_6.

On the other hand, high-temperature spectra were recorded for adduct **A-1** in DMSO-d_6. In particular, at +120 °C, the signals for the aromatic hydrogen atoms in the aniline-type ring changed from an ABCD system (8.18, 8.18, 7.85, 6.72 ppm at −60 °C) to a characteristic A_2B_2 pattern (8.04, 7.59 ppm) for a rapidly rotating *para*-substituted aromatic ring (Figure 9).

In the case of *p*-chloro-substituted adduct **A-2**, at room temperature (T = 20 °C), the four aromatic protons at the aniline-type aromatic ring are lost in the baseline owing to a coalescence process. When the temperature was lowered to −10 °C, the appearance of broad signals at 7.84, 7.01 ppm and 6.52 ppm was observed. Each one of these signals integrated for one proton. As the temperature was further lowered, the definition of these signals improved considerably. These signals sharpened at lower temperature, giving rise to three doublets with a coupling constant of *ca.* 8 Hz at −60 °C (Figure 10). On the other hand, when the sample was heated to +30 °C, a broadening of signals was evident in the aromatic region of the spectrum, between 7.4 ppm and 7.2 ppm, that eventually led to the appearance of two signals at 7.23 and 7.30 ppm at T = +120 °C (Figure 11).

In this context, variable-temperature C-13 NMR spectra of *p*-chloro-substituted adduct **A-2** exhibited similar spectroscopic behavior, giving rise to an average of signals for the *meta* and

Variable-temperature NMR spectroscopy

Nuclear magnetic resonance spectra were recorded at low temperature to establish the chemical shifts and coupling patterns of representative signals below coalescence. In the case of *p*-nitro-substituted adduct **A-1**, the room-temperature spectrum (20 °C) shows a simple signal at 8.05 ppm that integrates for two protons. When the temperature was lowered to −20 °C, this signal became very broad, essentially disappearing in the baseline, indicating that the coalescence temperature had been reached. Upon further cooling to −30 °C, the signal reappeared slightly upfield at 7.87 ppm. Additionally, a new signal was evident at 6.63 ppm, integrating for one proton. This signal sharpened at lower temperature (Figure 8).

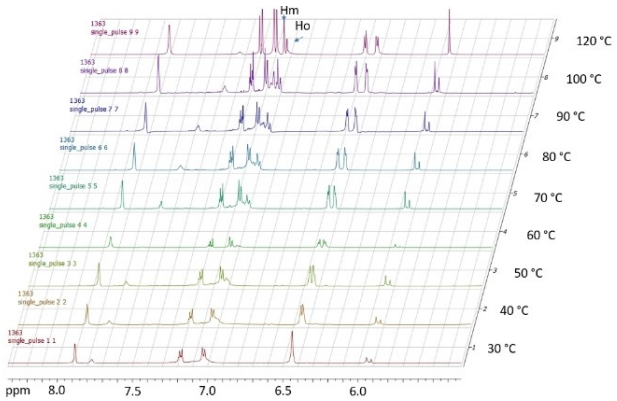

Figure 9. Variable-temperature H-1 NMR spectra for *p*-nitro-substituted adduct **A-1** at high temperature obtained in DMSO-d_6.

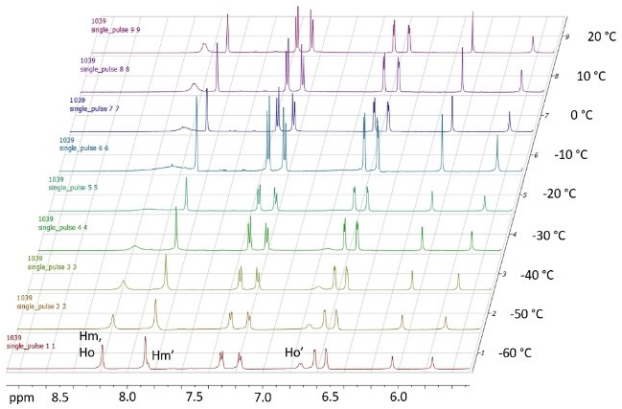

Figure 8. Variable-temperature H-1 NMR spectra for *p*-nitro-substituted adduct **A-1** at low temperature obtained in CD_2Cl_2.

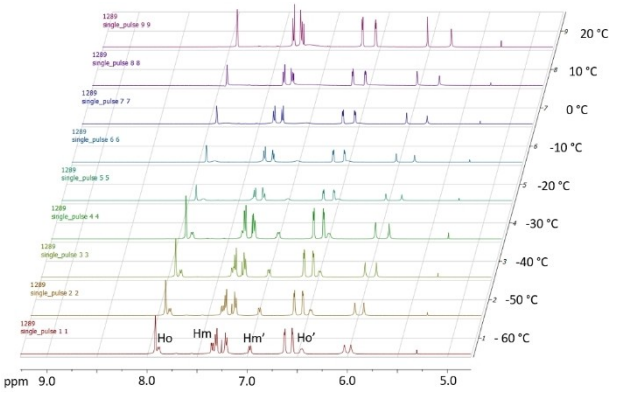

Figure 10. Variable-temperature H-1 NMR spectra for *p*-chloro-substituted adduct **A-2** at low temperature obtained in $CDCl_3$.

© 2022 The Authors. Published by Wiley-VCH GmbH

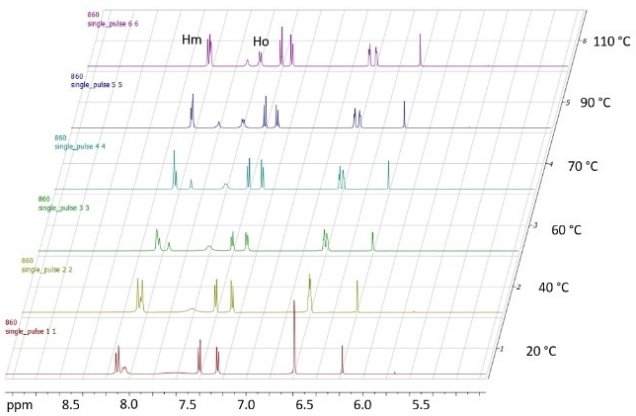

Figure 11. Variable-temperature H-1 NMR spectra for *p*-chloro-substituted adduct **A-2** at high temperature obtained in DMSO-d_6.

para carbons at +120 °C, whereas at room temperature the C-13 NMR signals became quite broad, to finally at −60 °C allow for the differentiation of all the carbons at the aromatic ring of the aniline portion, with chemical shifts δ = 133.0, 132.1, 130.0, 129.1 ppm (Figure 12).

The dynamic behavior described above for the H-1 and C-13 NMR signals corresponding to the nuclei in the aniline-type aromatic ring can be easily explained in terms of hindered rotation around the C–N bond leading to atropisomerism[23–25] (Scheme 4).

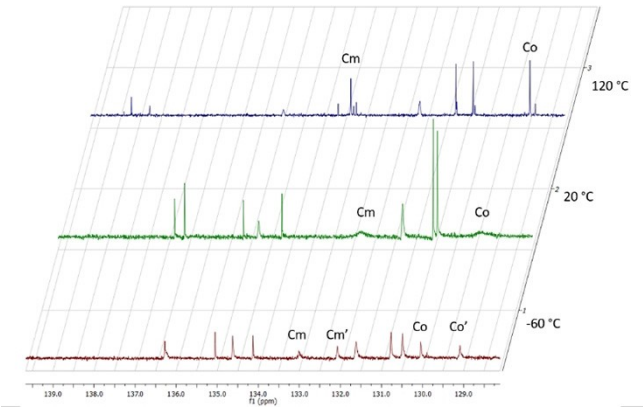

Figure 12. Variable-temperature C-13 NMR spectra of *p*-chloro-substituted adduct **A-2**, at −60 °C ($CDCl_3$), 20 °C ($CDCl_3$) and 120 °C (DMSO-d_6).

Scheme 4. Representation of hindered rotation around of the C–N bond in adducts **A-1** and **A-2**. The square represents the *t*-butyl-containing amide segment, the triangle represents the BODIPY moiety, and the circle represents the chloroacetyl fragment.

X-ray crystallographic diffraction analysis of BODIPY Ugi adduct A-1

Figure 13 depicts the structure obtained by X-ray diffraction analysis of BODIPY Ugi adduct **A-1**,[27] which corresponds to the anticipated molecule. A salient observation is the nearly coplanar orientation of the six-membered aromatic rings in the BODIPY moiety, with a dihedral angle θ = 28.03°. It can also be appreciated that both amide segments are oriented away from the six-membered aromatic rings, which discards potential hydrogen-bonding interactions in the solid state.

Molecular modeling and DFT calculations

Lowest energy conformations for BODIPY Ugi adducts **A-1** and **A-2** were calculated by means of DFT method with the B3LYP functional and the 6-31G(*d*) basis set.[28–31]

In the case of *p*-nitro-substituted adduct **A-1**, the lowest energy gas-phase conformation is the one shown in Figure 14. A salient observation is that, in contrast to the solid-state structure determined by X-ray diffraction crystallography, the phenyl ring on the BODIPY segment and the aniline-type aromatic ring adopt a nearly perpendicular, "T"-type arrangement, whereas the crystal structure presents a rather parallel arrangement between those aromatic rings (compare Figures 13 and 14). Importantly, this calculated optimized conformation helps explain the experimental NMR measurements exhibiting a rather large difference in chemical shifts

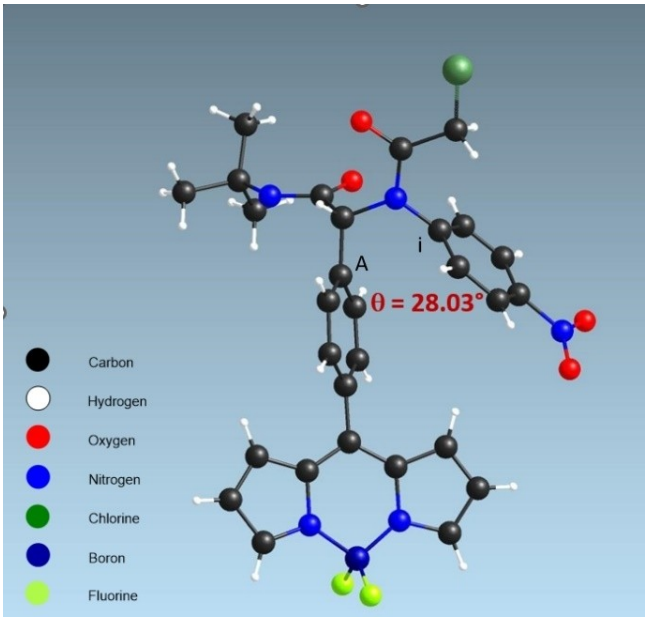

Figure 13. Structure and conformation of adduct **A-1** obtained by X-ray diffraction analysis.[27]

© 2022 The Authors. Published by Wiley-VCH GmbH

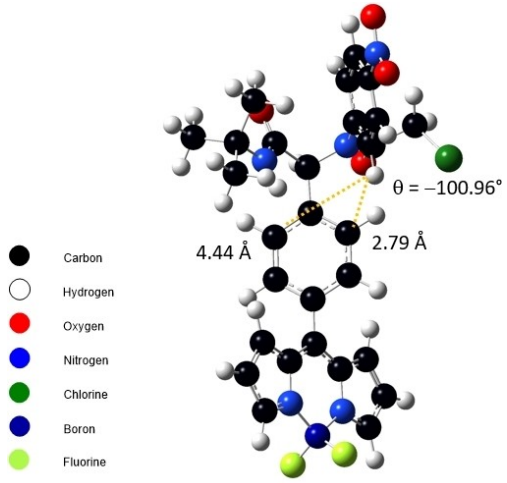

Figure 14. DFT-calculated (B3LYP functional and 6-31G(*d*) basis set) lowest energy conformer for **A-1**.

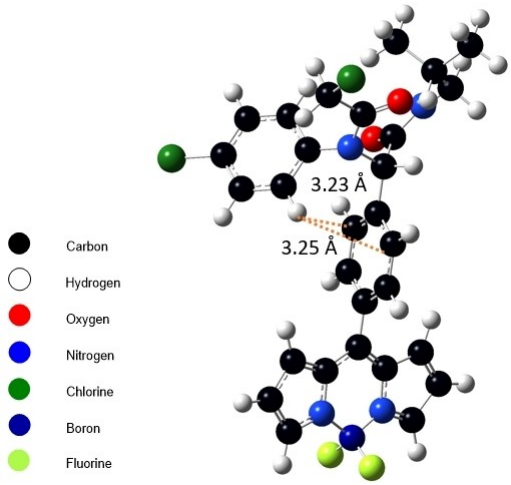

Figure 15. DFT-calculated (B3LYP functional and 6-31G(*d*) basis set) lowest energy conformation for **A-2**.

($\Delta\delta = 1.45$ ppm) for the *ortho* hydrogen atoms in the aniline-type ring. Indeed, the calculated distances between one *ortho* hydrogen atom on the aniline-type ring and the B carbon atoms on the BODIPY's bridging phenyl ring amount to 2.79 Å and 4.44 Å (Figure 14), suggesting that such a hydrogen atom is situated in the protecting anisotropic cone, in line with the significant upfield shift of $\delta = 6.72$ ppm. By contrast, the *ortho* hydrogen atoms do not fall within such shielding cone and present a typical $\delta = 8.17$ ppm chemical shift for an aromatic proton.

In the case of *p*-chloro-substituted BODIPY Ugi adduct **A-2**, the minimum energy conformer obtained through DFT calculations, showed an even greater proximity of one *ortho* hydrogen atom on the aniline-type aromatic ring to the shielding anisotropic cone of the phenyl ring of the BODIPY moiety. Indeed, the estimated distances between such an *ortho* hydrogen atom and the B carbons on the phenyl ring are 3.25 Å and 3.23 Å (Figure 15).

Conclusions

The conformational behavior of two novel BODIPY Ugi adducts **A-1** and **A-2** was investigated by variable-temperature NMR spectroscopy, X-ray diffraction analysis and DFT quantum mechanical calculations. Hindered rotation about the C–N bond of the aniline-type aromatic ring gives rise to a rather interesting dynamic process where some signals are broad and tend to vanish in the baseline at the coalescence temperature, $T = 20\,°C$. Low-temperature NMR spectra allow for the detection and assignment of all hydrogen and carbon atoms. By contrast, high-temperature NMR spectra give rise to averaged signals, when rotation about the C–N bond is rapid. A theoretical (DFT) study afforded the lowest energy conformations for BODIPY Ugi adducts **A-1** and **A-2**, which help understand the experimentally observed atypical chemical shifts for the protons on the aniline-type aromatic ring. In particular, crystal packing effects seem to be responsible for the nearly parallel orientation of the six-membered aromatic rings in the solid state, whereas gas-phase calculations indicate that a "T"-type arrangement between those aromatic rings is preferred in the gas phase. Structurally related Ugi adducts not containing the BODIPY do not exhibit the remarkable dynamic effect that is observed in **A-1** and **A-2**. This finding suggests that the BODIPY fragment is responsible of the peculiar conformational behavior reported herein.

Experimental Section

General Information

All ^{1}H and ^{13}C NMR spectra were recorded on a JEOL ECA 500 (500 MHz) spectrometer in deuterated chloroform ($CDCl_3$), deuterated dichloromethane (CD_2Cl_2) and deuterated dimethyl sulfoxide (DMSO-d_6) with tetramethylsilane (TMS) (0.00 ppm in H-1 spectra, 0.00 ppm C-13 spectra) or chloroform (7.26 ppm in H-1 spectra or 77.00 ppm in C-13 spectra) as internal reference. NMR data are reported in the following order: chemical shift in ppm, multiplicities (br (broad), s (singlet), d (doublet), t (triplet), q (quartet), m (multiplet), coupling constants, *J* (Hz), and integration. High-Speed Ball-Milling (HSBM) reactions were carried out in a Retsch Mixer Mill (MM200). TLC was conducted in silica gel on TLC Al foils. All reagents were purchased from Sigma-Aldrich (Merck) and used as received. Starting material 8-methylthio-BODIPY was purchased from Cuántico de México.

N-(*tert*-Butyl)-2-(2-chloro-*N*-(4-nitrophenyl)acetamido)-2-(4-(5,5-difluoro-5H-4 l4,5 l4-dipyrrolo[1,2-c:2′,1′-f][1,3,2]diazaborinin-10-yl)phenyl)acetamide, **A-1**. In a vial was placed formyl-BODIPY (40 mg, 0.14 mmol, 1 equiv.), *p*-nitroaniline (56 mg, 0.4053 mmol, 3 equiv.), chloroacetic acid (38.9 mg, 40.53 mmol, 3 equiv.), and 0.8 mL CH_2Cl_2. Next, *t*-butyl isocyanide (46.8 μL, 40.53 mmol, 3 equiv.), and 0.8 mL of distilled water were added to the vial and the resulting mixture was stirred for 24 h. The crude product was extracted with CH_2Cl_2 and concentrated for further purification by flash chromatography using Hex:EtOAc (1:1) as mobile phase. Dark orange solid, 32.8 mg, 41% yield. ^{1}H NMR (400 MHz, DMSO-d_6, $T = 20\,°C$) δ: 8.09 (d, $J = 5.3$ Hz, 2H), 7.95 (s, 2H), 7.41 (d, $J = 7.9$ Hz, 2H), 7.25 (d, $J = 7.9$ Hz, 2H), 6.60 (d, $J = 4$ Hz, 2H), 6.53 (d, $J = 3$ Hz, 2H),

© 2022 The Authors. Published by Wiley-VCH GmbH

6.05 (s, 1H), 5.65 (s, 1H), 3.84 (2d, $J=15$ Hz, 2H), 1.28 (s, 9H) ppm. ^{13}C NMR (100 MHz, DMSO-d_6) δ: 167.4, 166.2, 147.6, 145.4, 144.8, 144.1, 136.0, 134.6, 134.5, 132.2, 130.9, 130.7, 130.2, 124.2, 119.0, 65.3, 52.3, 41.9, 28.7 ppm.

N-(*tert*-Butyl)-2-(2-chloro-*N*-(4-chlorophenyl)acetamido)-2-(4-(5,5-difluoro-5H-4 l4,5 l4-dipyrrolo[1,2-c:2′,1′-f][1,3,2]diazaborinin-10-yl)phenyl)acetamide, **A-2**. In a vial were placed formyl-BODIPY (40 mg, 0.14 mmol, 1 equiv.), *p*-chloroaniline (52.8 mg, 0.41 mmol, 3 equiv.), chloroacetic acid (38.9 mg, 40.53 mmol, 3 equiv.), and 0.8 mL of CH_2Cl_2. Next, *t*-butyl isocyanide (46.8 µL, 40.53 mmol, 3 equiv.), and 0.8 mL of distilled water were added to the reaction vial. The resulting mixture was stirred for 24 h and the crude product was extracted with CH_2Cl_2 and concentrated for further purification by flash chromatography using Hex:EtOAc (1:1) as mobile phase. Dark red solid, 17 mg, 35% yield. ^{1}H NMR (400 MHz, $CDCl_3$) δ: 7.95 (s, 2H), 7.40–7.29 (m, 4H), 6.71 (d, $J=4$ Hz, 2H), 6.57 (d, $J=4$ Hz, 2H), 6.05 (s, 1H), 5.81 (s, 1H), 3.89 (m, 2H), 1.42 (s, 9H) ppm. ^{13}C NMR (100 MHz, $CDCl_3$) δ: 167.8, 166.8,145.9, 144.5, 136.8, 136.5, 135.1, 134.7, 134.2, 132.2, 131.2, 130.5, 130.3, 129.3, 118.9, 65.2, 52.1, 42.3, 28.7 ppm.

Acknowledgements

The authors are indebted to CONACYT for research grant A1-S-44097, and to Fund SEP-CINVESTAV for grant No. 126. G. G.-V. is grateful to CONACYT for scholarship 1004082 and I. J. A.-C. thanks CONACYT for postdoctoral grant 849322. We thank Dr. Mario Pérez-Venegas for helpful advice and Carlos Naranjo-Castañeda for technical assistance. We are also grateful to Laboratorio Nacional de la Ugto for giving us access to the computational facilities.

Conflict of Interest

The authors declare no conflict of interest.

Data Availability Statement

The data that support the findings of this study are available in the Supporting Information of this article.

Keywords: BODIPY · dynamic conformational processes · hindered rotation · Ugi adducts · VT NMR spectroscopy

[1] A. Loudet, K. Burguess, *Chem. Rev.* **2007**, *107*, 4891–4932.
[2] R. Ziessel, G. Ulrich, A. Harriman, *New J. Chem.* **2007**, *31*, 496–501.
[3] C. A. Benniston, G. Copley, *Phys. Chem. Chem. Phys.* **2009**, *11*, 4124–4131.
[4] T. E. Wood, A. Thompson, *Chem. Rev.* **2007**, *107*,1831–1861.
[5] S. Kolemen, E. U. Akkaya, *Coord. Chem. Rev.* **2018**, *354*, 121–134.
[6] N. Boens, V. Leen, W. Dehaen, *Chem. Soc. Rev.* **2012**, *41*, 1130–1172.
[7] W. Zhang, A. Ahmed, H. Cong, S. Wang, Y. Shen, B. Yu, *Dyes Pigm.* **2021**, *185*,108937.
[8] A. Bessette, G. S. Hanan, *Chem. Soc. Rev.* **2014**, *43*, 3342–3405.
[9] P. M. Gurubasavaraj, V. P. Sajjan, B. M. Muñoz-Flores, V. M. Jiménez Pérez, N. S. Hosmane, *Molecules* **2022**, *27*, 1877.
[10] L. S. Liebeskind, J. Srogl, *J. Am. Chem. Soc.* **2000**, *122*, 11260–11261.
[11] E. Peña-Cabrera, A. Aguilar-Aguilar, M. González-Domínguez, E. Lager, R. Zamudio-Vázquez, J. Godoy-Vargas, F. Villanueva-García, *Org. Lett.* **2007**, *9*, 3985–3988.
[12] E. Lager, J. Liu, A. Aguilar-Aguilar, B. Z. Tang, E. Peña-Cabrera, *J. Org. Chem.* **2009**, *74*, 2053–2058.
[13] J. Han, O. Gonzalez, A. Aguilar-Aguilar, E. Peña-Cabrera, K. Burgess, *Org. Biomol. Chem.* **2009**, *7*, 34–36.
[14] I. J. Arroyo, R. Hu, B. Z. Tang, F. I. López, E. Peña-Cabrera, *Tetrahedron* **2011**, *67*, 7244–7250.
[15] M. Pérez-Venegas, M. N. Villanueva-Hernández, E. Peña-Cabrera, E. Juaristi, *Organometallics* **2020**, *39*, 2561–2564.
[16] S. Shaabani, A. Doemling, *Angew. Chem. Int. Ed.* **2018**, *57*, 16266–16268; *Angew. Chem.* **2018**, *130*, 16502–16504.
[17] R. C. Cioc, E. Ruijter, R. V. A. Orru, *Green Chem.* **2014**, *16*, 2958–2975.
[18] D. A. Contreras-Cruz, M. A. Sánchez-Carmona, F. A. Vengoechea-Gómez, D. Peña-Ortiz, L. D. Miranda, *Tetrahedron* **2017**, *73*, 6146–6156.
[19] M. G. Ricardo, A. V. Vasco, D. G. Rivera, L. A. Wessjohann, *Org. Lett.* **2019**, *21*, 7307–7310.
[20] J. C. Flores-Reyes, A. Islas-Jacome, E. González-Zamora, *Org. Chem. Front.* **2021**, *8*, 5460–5515.
[21] L. A. Polindara-García, E. Juaristi, *Eur. J. Org. Chem.* **2016**, *2016*, 1095–1102.
[22] M. Pérez-Venegas, T. Arbeloa, J. Bañuelos, I. López-Arbeloa, N. E. Lozoya-Pérez, B. Franco, H. M. Mora-Montes, J. L. Belmonte-Vázquez, C. I. Bautista-Hernández, E. Peña-Cabrera, E. Juaristi, *Eur. J. Org. Chem.* **2021**, *2021*, 253–265.
[23] D. Homma, S. Taketani, T. Shirai, E. Caytan, C. Rouesel, J. Elguero, I. Alkorta, O. Kitagawa, *J. Org. Chem.* **2022**, *87*, 8118–8125.
[24] J. E. Díaz, A. Mazzanti, L. R. Orelli, M. Mancinelli, *ACS Omega* **2019**, *4*, 4712–4720.
[25] R. Costil, A. J. Sterling, F. Duarte, J. Clayden, *Angew. Chem. Int. Ed.* **2020**, *59*, 18670–18678; *Angew. Chem.* **2020**, *132*, 18829–18837.
[26] C.-P. Dong, A. Uematsu, S. Kumazawa, Y. Yamamoto, S. Kodama, A. Nomoto, M. Ueshima, A. Ogawa, *J. Org. Chem.* **2019**, *84*, 11562–11571.
[27] Deposition Numbers 2183214 and 2183215 (for **A-1**) contain the supplementary crystallographic data for this paper. These data are provided free of charge by the joint Cambridge Crystallographic Data Centre and Fachinformationszentrum Karlsruhe Access Structures service.
[28] A. D. Becke, *Phys. Rev. A* **1988**, *38*, 3098–3099.
[29] C. Lee, W. Yang, R. G. Parr, *Phys. Rev. B* **1988**, *37*, 785–789.
[30] Q. Wu, W. Yang, *J. Chem. Phys.* **2002**, *116*, 515–524.
[31] D. Cassarini, L. Lunazzi, A. Mazzanti, *Eur. J. Org. Chem.* **2010**, *11* 2035–2056.

Manuscript received: September 9, 2022
Revised manuscript received: September 22, 2022

© 2022 The Authors. Published by Wiley-VCH GmbH